An Sfi1-like centrin-interacting centriolar plaque protein affects nuclear microtubule homeostasis.

Christoph Wenz[1+], Caroline S. Simon[1+#], Tatiany Patricia Romão[1,§], Vanessa Stürmer[1], Marta Machado[1], Natacha Klages[2], Anja Klemmer[1], Yannik Voß[1], Markus Ganter[1], Mathieu Brochet[2], Julien Guizetti[1*]

[1] Center for Infectious Diseases, Heidelberg University Hospital, 69120 Heidelberg, Germany

[2] Department of Microbiology and Molecular Medicine, Faculty of Medicine, University of Geneva, CH-1211 Geneva, Switzerland.

[§] current address: Department of Entomology, Instituto Aggeu Magalhães-FIOCRUZ, Recife 50740-465, PE, Brazil.

[#] current address: European Molecular Biology Laboratory, Advanced Light Microscopy Facility, Heidelberg, Germany.

[+] those authors contributed equally

* Correspondence: julien.guizetti@med.uni-heidelberg.de

Abstract

Malaria-causing parasites achieve rapid proliferation in human blood through multiple rounds of asynchronous nuclear division followed by daughter cell formation. Nuclear divisions critically depend on the centriolar plaque, which organizes intranuclear spindle microtubules. The centriolar plaque consists of an extranuclear compartment, which is connected via a nuclear pore-like structure to a chromatin-free intranuclear compartment. Composition and function of this non-canonical centrosome remain largely elusive. Centrins, which reside in the extranuclear part, are among the very few centrosomal proteins conserved in *Plasmodium falciparum*. Here we identify a novel centrin-interacting centriolar plaque protein. Conditional knock down of this Sfi1-like protein (PfSlp) caused a growth delay in blood stages, which correlated with a reduced number of daughter cells. Surprisingly, intranuclear tubulin abundance was significantly increased, which raises the hypothesis that the centriolar plaque might be implicated in regulating tubulin levels. Disruption of microtubule homeostasis caused polymerization of excess microtubules and aberrant mitotic spindles. Time-lapse microscopy revealed that this prevented or delayed spindle extension. Our study thereby identifies a novel extranuclear centriolar plaque factor and establishes a functional link to the intranuclear compartment of this divergent eukaryotic centrosome.

Introduction

Cell division drives the expansion of life, which includes infectious pathogens, such as *Plasmodium falciparum* that proliferate in the blood of their human host. This parasite can thereby cause malaria which still results in more than 600,000 deaths per year [1]. Multiplication within the red blood cell that is invaded by the intracellular parasite is driven by an atypical cell division mode, called schizogony [2,3]. The start of schizogony is not precisely defined but occurs around 28 hours post invasion (hpi) once *P. falciparum* has gone through the preceding ring and trophozoite stage. Schizogony consists of multiple rounds of nuclear division without cytokinesis yielding between 8 to 30 nuclei. At about 44 hpi those nuclei are packed into the daughter merozoites that egress from their host cell after about 48 hpi. How the parasite “decides” when the final number of nuclei is reached is unclear, but some studies suggest an implication of nutrients [4–6]. These cycles of nuclear division, merozoite formation, egress, and reinvasion can result in the high parasitemias that are associated with severe disease progression [7].

Our understanding of cell division in *Plasmodium* spp. is increasing but due to the high divergence from model organisms many of the underlying molecular mechanisms are remaining unclear [8,9]. Notable differences are the autonomous nuclear cycles of DNA replication, chromosome segregation, and division [10,11]. During this process chromosomes are not condensed, and the nuclear envelope remains intact. The lack of a genetically encoded nuclear envelope marker has limited a more detailed study of karyofission but recent adaptation of membrane staining will allow progress in this domain [12,13]. Classical components of cell cycle regulatory pathways, such as cyclins, kinases, and phosphatases, are significantly less conserved [8,9,14–20].

Whether cell cycle checkpoints similar to the ones described in model organisms exist in the malaria-causing parasite is still debated [21–24]. The observation that drug-mediated depolymerization of microtubules, which would trigger a spindle assembly checkpoint, does not cause a noticeable delay in DNA replication has been interpreted as the absence of this checkpoint [23,25]. Depletion of components of the mini-chromosome maintenance complex despite leading to aberrant spindles has also been speculated not to trigger a checkpoint [26]. Conclusive and time-resolved data showing an inducible and reversible delay in cell cycle progression, which is necessary to demonstrate a checkpoint, is missing to date. Taken together there is a need to identify more of the players involved in parasite proliferation and generate additional highly resolved, quantitative cell biological data.

A key effector of nuclear division during schizogony is the centriolar plaque (CP), the centrosome of *P. falciparum*. In mammals, centrosomes act as microtubule organizing centers (MTOC) and need to duplicate only once per cell cycle [27]. The CP of asexual blood

stage parasites multiplies once each nuclear cycle and contains very few conserved centrosomal proteins [28–30]. The CP serves as a nucleation site for nuclear microtubules, while cytoplasmic microtubules are absent in schizonts [3,31–34]. Prior to the first nuclear division a monopolar spindle, also called hemispindle, with 2-11 long microtubules radiating from the intranuclear compartment of the CP, is formed [34,35] (Fig. 1A). Shortly thereafter centrin, the only currently known extranuclear CP marker, is recruited [34,36,37]. Centrins are a group of calcium binding proteins that are associated with virtually all eukaryotic centrosomes and have been implicated in their duplication [28,38,39]. A key interaction partner of centrin in most organisms is Sfi1 and the presence of an orthologue has been hypothesized for *P. falciparum* [29,40–42]. Shortly after centrin recruitment the hemispindle collapses, the centrin signal duplicates and the mitotic spindle assembles [34]. The first nuclear division is concluded by segregation of replicated chromosome sets by an extending spindle and karyofission [12]. Subsequent asynchronous nuclear division cycles lead to a multinucleated schizont (Fig. 1A).

How intranuclear microtubule dynamics are regulated in malaria parasites is unclear, but several microtubule motor proteins have been described [43,44]. Tubulin polymerization into microtubules is a concentration-dependent effect [45–47], which led us to hypothesize that hemispindle formation is an effect of high nuclear tubulin concentration [34]. How nuclear tubulin homeostasis is regulated is currently unknown.

In this study, we identify a novel centrin-interacting protein in the outer centriolar plaque and possible orthologue of Sfi1. Its knock down causes an increase in intranuclear microtubules, implicating the outer CP in regulation of tubulin homeostasis. Using time-lapse microscopy, we reveal important delays in the elongation of aberrant spindles that could be explained by a spindle assembly checkpoint.

Results

To identify novel components of the centriolar plaque we carried out co-immunoprecipitation on a *P. falciparum* 3D7 strain episomally expressing PfCen1-GFP using a GFP-antibody without prior protein crosslinking (Fig. S1). Mass spectrometry analysis of the eluate revealed 11 proteins (Table S1), of which 8 can also frequently be identified in a GFP control pulldown [48]. Within the three specific hits we found, beside PfCen1 itself and PfCen3, a protein of unknown function, PF3D7_0710000. The interaction with another centrin is consistent with previous findings in *P. berghei* [37]. PF3D7_0710000 is a weakly expressed and highly essential protein [49], with a size of 407kDa and was previously hypothesized to be a functional orthologue of Sfi1 [29]. This prediction was based on the presence of multiple centrin-binding consensus motifs. Our own sequence analysis using a minimal centrin-binding motif, [FLW]XXW[KR] [50], indeed shows the accumulation of those motifs within Sfi1 proteins of divergent species (Fig. 1B) and revealed that PF3D7_0710000 has the highest number of centrin binding motifs of all *P. falciparum* proteins. Therefore, we decided to name PF3D7_0710000 the Sfi1-like protein (PfSlp). To localize PfSlp, we integrated an endogenous C-terminal GFP tag using selection-linked integration [51] (Fig. 1C). Additionally, we added a *glmS* ribozyme sequence to enable glucosamine (GlcN)-mediated knock down of *PfSlp* mRNA [52]. Correct integration was validated by PCR (Fig. S2). The resulting 3D7_pSLI_PfSlp-GFP_*glmS* parasite line will hereafter be referred to as ‘Slp’. Due to its low expression PfSlp-GFP was not directly detectable in live cells. Immunofluorescence staining with an anti-GFP antibody, however, revealed a specific signal within the outer centriolar plaque as indicated by colocalization with centrin at the spindle poles (Fig. 1D). Even at the increased spatial resolution of STED microscopy PfSlp signal was proximal to centrin, corroborating their direct interaction. Ring and trophozoite stages did not show any PfSlp signal (Fig. S3). Upon transition into schizogony late trophozoites develop a hemispindle in their nucleus of which about half carry a centrin signal [34] (Fig. 1A). Our co-staining of PfSlp in those stages showed that 24 out of 25 centrin-positive centriolar plaques also had a PfSlp signal, while 24 out of 26 PfSlp-positive centriolar plaques also showed centrin (Fig. 1E) indicating that both proteins are recruited together or at least simultaneously.

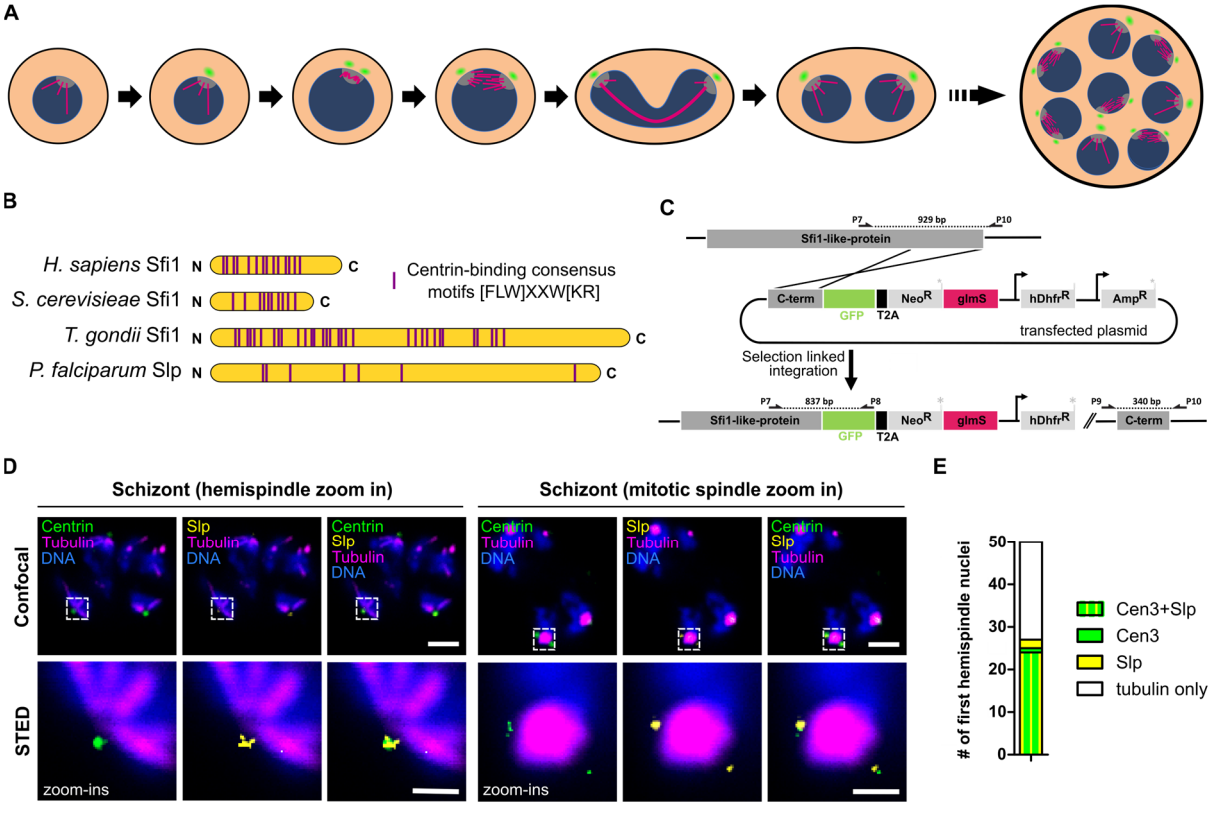

Figure 1. The Sfi1-like protein (PfSlp) co-localizes with centrin at the centriolar plaque. A) *Schematic of first nuclear division in Plasmodium falciparum during blood stage schizogony (red blood cell not shown). After polymerization of hemispindle microtubules (magenta) at the inner core of the CP (grey), centrin (green) is recruited to the outer core of the CP. The centriolar plaque is duplicated, and the mitotic spindle is formed. During anaphase chromosomes (blue) are segregated and two nuclei are formed. Subsequent asynchronous nuclear division cycles lead to a multinucleated cell stage, which later gives rise to multiple daughter cells.* ***B)*** *Schematic comparison of human, Saccharomyces cerevisiae, and Toxoplasma gondii Sfi1 with* PfSlp. *No clear sequence homology to other Sfi1 proteins exists, but multiple centrin-binding site consensus motifs can be identified.* ***C)*** *Endogenous* PfSlp *tagging strategy with GFP and glmS ribozyme via selection-linked integration (SLI).* ***D)*** *Confocal microscopy images of immunofluorescence staining of blood stage schizont expressing endogenously tagged PfSlp-GFP using anti-centrin (green), anti-tubulin (magenta), anti-GFP (yellow) antibodies, and DNA stained with Hoechst (blue). Dual-color STED zoom-ins with super-resolved PfSlp-GFP and centrin signal. Maximum intensity projections are shown for confocal images. Scale bars, confocal, 1.5 µm; STED, 0.5 µm.* ***D)*** *Quantitative analysis of PfSlp, centrin and tubulin immunostained parasites in mononucleated schizonts with hemispindle. CPs were scored for presence (27/50) and absence (23/50) of centrin and/or PfSlp signal.*

To investigate the function of this novel centriolar plaque component we induced conditional self-cleavage of PfSlp-GFP_*glmS* mRNA by treatment of rings with 3.5 mM GlcN. After 73 h we measured a 55% reduction in steady state PfSlp mRNA levels by qPCR (Fig. 2A). This could be recapitulated by a significantly reduced PfSlp-GFP signal at the centriolar plaque measured in immunostained cells (Fig. S4). Endogenous centrin levels at the centriolar plaque were also reduced (Fig. 2B), affirming that PfSlp and centrin are part of one complex and that centrin recruitment partly depends on PfSlp. GlcN treatment further caused a growth defect over several cycles (Fig. 2C). Although GlcN also influenced growth of 3D7 wild type

(wt), as described previously [53], the growth defect was markedly stronger in the Slp line. Analysis of the distribution of developmental stages of Giemsa-stained parasites showed a delay at the trophozoite to schizont transition in the first cycle in GlcN treated Slp cells, which however was less pronounced in the second life cycle (Fig. S5). To test whether DNA replication kinetics were altered we analysed RNase-treated, SYBR-stained cultures by flow cytometry while progressing through the first schizogony after GlcN addition (Fig. 2D). Both untreated Slp and 3D7 showed a peak DNA signal intensity at 42 hpi. GlcN treatment caused a slight shift in replication onset, while DNA peak intensity was reached later in Slp +GlcN, suggesting delayed schizogony. The reduction in merozoite number specifically in GlcN-treated Slp parasites corroborates a defect in schizogony including nuclear division (Fig. 2E).

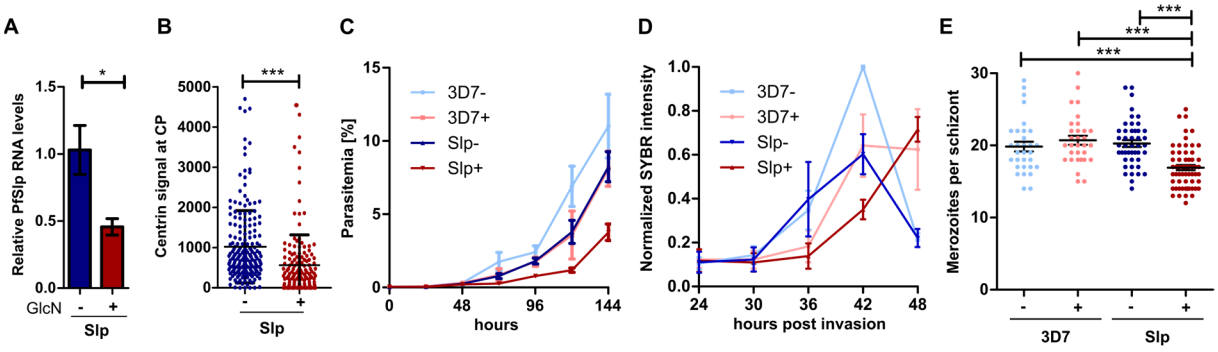

Figure 2. PfSlp knock down impedes parasite growth and nuclear multiplication. A) *Real time qPCR analysis of PfSlp mRNA levels in Slp parasite line treated with 3.5 mM GlcN for 73h (+) or left untreated (-). Serine-tRNA ligase was used as control gene. N=3. Statistical analysis: t-test with Welch´s correction.* ***B)*** *Relative fluorescence signal intensity of centrin signal at the centriolar plaque was measured in +/-GlcN Slp schizont parasites with up to 10 nuclei immunostained as in Fig. 1D.* ***C)*** *Growth curves of 3D7 wild type and Slp strain +/- GlcN. Parasitemia was measured via flow cytometry after SYBR-Green staining and fixation for 6 days after treatment. N=3.* ***D)*** *Flow cytometry analysis of SYBR-Green stained and RNase treated 3D7 and Slp parasites +/-GlcN indicating changes in DNA replication. N=3. Intensity normalized to 3D7 -GlcN 42 hpi.* ***E)*** *Giemsa-based merozoite counting of late stages schizonts +/-GlcN. Egress inhibitor E64 was added at 50µM for 4h at the end of schizogony before analysis of segmenters. 3D7 +/-GlcN (n=31/31), Slp +/-GlcN (n=62/45). Statistical analysis: t-test with Welch´s correction.*

Since the defect in nuclear division was specific to PfSlp knock down rather than GlcN treatment (Fig. 2D) we analysed the microtubule organization in Slp +/- GlcN parasites by immunofluorescence staining (Fig. 3). Nuclei with hemispindles contained more prominent microtubule branches in GlcN-treated cells (Fig. 3A). Indeed, quantification of the cumulative microtubule length per hemispindle in schizonts revealed a significant increase upon PfSlp knock down (Fig. 3B). Individual microtubules cannot be distinguished in mitotic spindle stage nuclei, but the overall tubulin signal intensity was high, and we frequently observed microtubule protrusions in GlcN treated parasites, while normal mitotic spindles have a very consistent ovoid shape (Fig. 3C). Since the nucleoplasmic tubulin signal intensity was not above the cytoplasmic or extracellular background, we assume that the majority of

intranuclear tubulin is in the polymerized form. We therefore quantified the spindle-associated tubulin signal and found significantly higher abundance in GlcN-treated parasites for hemispindles and mitotic spindles, indicating a restrictive role of PfSlp in nuclear tubulin homeostasis (Fig. 3D). To investigate the cause of increased intranuclear tubulin we quantified the cellular tubulin pool by western blot analysis of total protein extract of Slp parasites at 24, 30, and 36 hpi +/- GlcN (Fig. S6A). Quantification of tubulin protein band intensity, normalized to differences in aldolase levels (Fig. S6B), revealed that total tubulin levels were not strongly increased in GlcN-treated parasite population while entering schizogony around 24-30 hpi (Fig. 3E). Actually, tubulin levels were lower in GlcN treated cells at 36 hpi, which could be explained by a delay in cell cycle progression (Fig. 2C & S5), which is more pronounced at this later stage. Taken together this renders the increase in nuclear tubulin through globally higher tubulin expression unlikely and rather suggests a redistribution of the tubulin pool. Additionally, we observed no strong differences in centrin protein band intensity between +/- GlcN (Fig. S6C), which could account for the different centrin levels observed at the centriolar plaque in PfSlp knock down conditions using IFA (Fig. 2B).

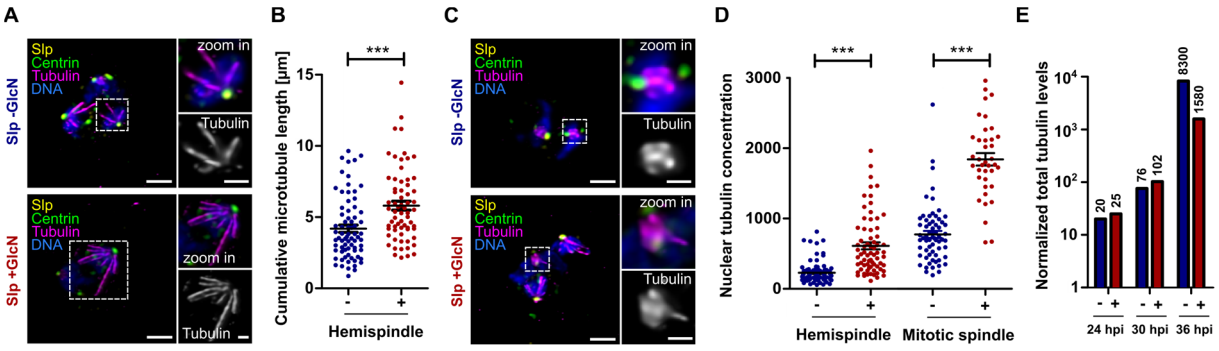

Figure 3. PfSlp knock down causes increase of intranuclear microtubule mass. A) *Lightning deconvolution confocal microscopy image of Slp strain schizont stained with anti-centrin (green), anti-tubulin (magenta), and anti-GFP (yellow) antibody. DNA stained with Hoechst (blue). Maximum intensity projections are shown. Hemispindles show extended microtubules in +GlcN condition (bottom) Scale: 1.5 µm, zoom ins: 0.5 µm.* ***B)*** *Quantification of cumulative microtubule branch length in Slp schizont parasites reveal a significant increase in +GlcN (n=66) vs -GlcN (n=73) parasites.* ***C)*** *Staining and image acquisition as in A) reveals aberrant mitotic spindles in Slp +GlcN schizonts that display protruding microtubule branches (bottom).* ***D)*** *Nuclear tubulin signal concentration was determined on images as seen in A) and C) using polygon selections for individual hemispindles or mitotic spindles in average intensity projections after nuclear and extracellular background subtraction. Hemispindles (-GlcN (n=91), +GlcN (n=70)), mitotic spindles (-GlcN (n=65), +GlcN (n=38)). Statistical analysis: t-test with Welch´s correction.* ***E)*** *Western blot analysis of whole cell lysate of synchronized Slp strain at 24, 30, and 36 hpi +/- GlcN using anti-tubulin antibody normalized to difference in aldolase levels and loaded parasites. Plotted on log scale. Absolute numbers indicated above bars.*

To quantify the effects of excessive nuclear tubulin abundance and errors in the mitotic spindle organization on division we used time-lapse imaging of parasites entering schizogony stained with a live-cell compatible microtubule dye, SPY555-Tubulin. In Slp -GlcN conditions

95% (n=18) of parasites successfully completed their first mitotic division, as indicated by full spindle elongation and duplication of the spindle signal (Fig. 4A, Mov. S1). Since replication kinetics suffered a slight GlcN-dependent delay we also analysed 3D7 +GlcN were also 95% (n=20) of cells extended their spindles (Fig. S7A, Mov. S2). Strikingly, in Slp +GlcN knock down parasites, only 53% (n=36) completed the first division, while the 47% of parasites, in which presumably the knock down was most effective, failed to do so often after several short spindle extensions and contractions (Fig. 4A, Mov. S3). For those cells which underwent spindle extension we quantified the duration of the mitotic spindle stages and observed a significant prolongation in Slp +GlcN cells (Fig. 4B) while Slp -GlcN and 3D7 +GlcN cells (Fig. S7B) showed a mitotic spindle phase duration consistent with previously published data [34]. To test if this delay is related to a perturbed microtubule quantity, we quantified the SPY555-Tubulin fluorescence intensity of the first mitotic spindle as soon as it formed and found an increased microtubule quantity in PfSlp knock down (Fig. S8). Taken together this study characterizes a novel possible Sfi1 orthologue, PfSlp, which interacts with centrin and plays a role in the homeostasis of nuclear tubulin during schizogony (Fig. 4C).

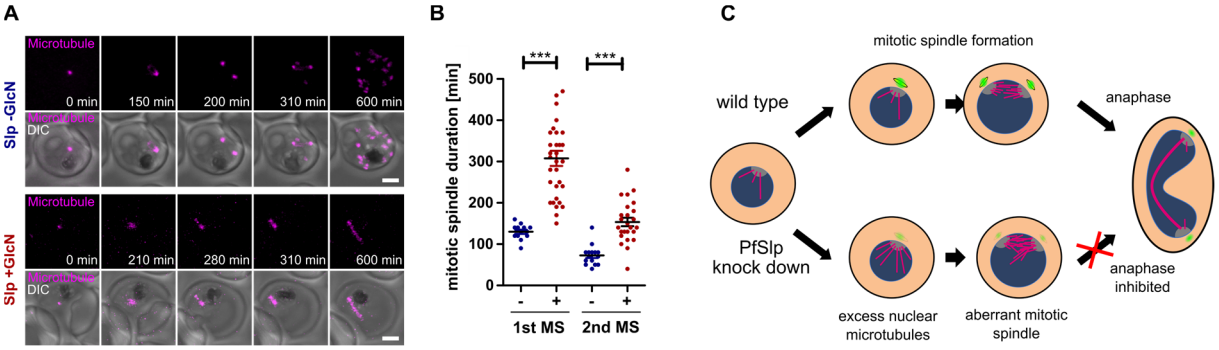

Figure 4. Increased nuclear tubulin abundance inhibits spindle extension. A) *Time-lapse confocal imaging of Slp +/-GlcN parasites undergoing schizogony stained with SPY555-Tubulin (magenta). Maximum intensity projections are shown. Scale bars, 1.5 µm.* ***B)*** *Quantification of first (Slp-GlcN (n=18), Slp +GlcN (n=31)) and second (Slp -GlcN (n=16), Slp +GlcN (n=25)) mitotic spindle stage duration using live-cell movies of tubulin-stained parasites that undergo spindle extension. Statistical analysis: t-test with Welch´s correction.* ***C)*** *Schematic model of function of the centrin/Slp complex in affecting proper mitotic spindle assembly.*

Discussion

Our PfCen1-GFP co-immunoprecipitation identified a very short list of hits, of which only PfSlp and PfCen3 were specific. Interaction between different centrins has been previously documented in *Plasmodium* [37]. The omission of cross-linking and PfSlp expression levels being relatively low, therefore implies a strong interaction that is corroborated by previously published yeast two-hybrid data [54]. While in confocal microscopy the PfSlp and centrin signals overlap completely we could occasionally see a small gap between signals in super-resolved STED images. In yeast, it was previously shown that the C- and N-terminus of yeast Sfi1, which has a highly elongated structure, are at a distance of 120 nm [40]. Given that the centrin binding motifs in PfSlp are more N-terminally located while the GFP-tag was placed at the C-terminus this gap can readily be explained by the large size of PfSlp.

The centrin-Sfi1 complex seems conserved throughout many eukaryotes and our findings support this for *Plasmodium* spp. [55]. In mammals Sfi1 localizes within centrioles and seems implicated in maintaining centriole architecture and cohesion [42]. Centrioles are however missing from the centriolar plaque of asexual blood stage parasites. A related structure in this context is the spindle pole body (SPB) of budding yeast, which also undergoes closed mitosis. In yeast, Sfi1 interacts with the yeast centrin homologue Cdc31 and is essential for duplication of the SPB [56]. Sfi1 is part of a structure called the half bridge, which binds Cdc31 and later rearranges into a full bridge by antiparallel binding to allow assembly of the second spindle pole [40,41,56–58]. Although we did not observe a specific defect in centriolar plaque duplication we are currently lacking independent centriolar plaque markers to investigate this question more directly. In *T. gondii,* a Sfi1 homologue was found in the outer core of the bipartite centrosome colocalizing with TgCentrin [29]. *T. gondii*, however carries centriole-like structures that could harbor the observed Sfi1 signal as evidenced by the colocalization with Sas-6, a canonical eukaryotic centriole component [28]. A temperature-sensitive TgSfi1 mutant had a loss of outer core duplication which was associated with a severe block in budding [29]. What the unifying functions of Sfi1 and centrin are in the context of these highly divergent centrosomal structures needs to be analyzed more extensively.

An impact on nuclear tubulin homeostasis, which is more relevant for organisms undergoing closed mitosis, has however not been described [59,60]. Higher intranuclear tubulin abundance can in principle be explained by a delay at the entry into schizogony caused e.g. by a failure to properly duplicate the centriolar plaque, which would then lead to an accumulation tubulin before progressing through mitosis. Since we excluded a global increase in tubulin levels in PfSlp knock down (Fig.3E), one could also hypothesize an effect on tubulin import into the nucleus. The positioning of PfSlp close to the neck of the centriolar

plaque which connects the extranuclear and intranuclear compartment raises the possibility that this specialized nuclear pore might be implicated in the import of division factors such as tubulin. This would allow the parasite to specifically regulate the nuclear levels of proteins required for DNA replication and chromosome segregation during schizogony.

Importantly, we observed that the majority of PfSlp knock down cells could not complete spindle extension while the ones that did progress were significantly delayed. This presents a very early phenotype that manifest right after recruitment of centrin and PfSlp to the centriolar plaque and is corroborated by an increase in microtubules in the first mitotic spindle as it forms (Fig. S8). This also explains the comparatively mild phenotypes at later stages, such as the only slightly decreased merozoite number (Fig. 2E) and the decrease in developmental stage delay (Fig. S5), as those might result from parasites for which the knock down was presumably less effective. The failure to properly progress through anaphase can be explained by the disorganization of the mitotic spindle, which relies on tightly regulated microtubule dynamics [61]. The lack of properly arranged interpolar microtubules could, e.g., reduce the pushing forces required for spindle extension. It is also plausible that proper kinetochore attachment and separation are disturbed under those conditions. If some type of spindle assembly checkpoint existed, as had been postulated in *T. gondii* [62], it could cause an anaphase delay, like the one observed in our data. The recent discovery of a Mad1 homolog in *Plasmodium* spp. further argues for the conservation of a spindle checkpoint in Apicomplexa [24]. By no means is this conclusive evidence for a mitotic checkpoint, which would among other things require the demonstration of reversibility. It, however, highlights the importance of time-resolved single-cell data, which was not available in previous studies implying the absence of a mitotic checkpoint [12,23,25,26].

Eukaryotic centrosomes remain fascinatingly diverse structures that use a mixture of common and divergent mechanisms that need to be investigated in more detail using evolutionary cell biology approaches.

Materials and Methods

Parasite culture

The *P. falciparum* 3D7 wild type cell line and the 3D7_SLI_slp-gfp_*glmS* (Slp) strain were cultured in 0+ human red blood cells using RPMI 1640 medium (Sigma) with added 0.2 mM hypoxanthine, 25 mM HEPES, 0.5% Albumax™ and 12.5 µg/ml Gentamicin (cRPMI) at a hematocrit of 2.5% and an average parasitemia of 1-5%. For washing of cells, cRPMI without Albumax was used (iRPMI). For Slp, 600ug/ml Geneticin-G418 (Thermo Fisher) were added. Parasites were incubated at 90% relative humidity, 5% O_2 and 3% CO_2 at 37°C. Parasites were synchronized by selective lysis of schizonts using 5% D-sorbitol for 10 minutes at 37°C, performed three times throughout one week.

Co-immunoprecipitation

Co-immunoprecipitation was based on previous work [20,63]. Specifically, 3.75 ml of NF54 PfCentrin1-GFP schizont culture were harvested at a parasitemia of circa 5%. Therefore, red blood cells were pelleted for 5 min at 340 g and lysed with 0.1% saponin/cRPMI for 1 min at room temperature. Lysed cells were pelleted (3000 g, 6 min) and washed with 0.1 % saponin/iRPMI by centrifugation (3000 g, 6 min). The following steps were performed on ice if not stated otherwise. For parasite lysis, the sample was incubated with 1 ml RIPA buffer (50 mM Tris-HCl, pH 8, 150 mM NaCl, 1% NP-40, 0.5% sodium deoxycholate, 0.1% SDS) freshly supplemented with 1 mM DTT and 1x protease inhibitor (Halt™ Protease Inhibitor Cocktail, 78430, Thermo Fisher Scientific) for 30 min. For mechanical homogenization, the sample was passed ten times through a needle (0.3 mm diameter) attached to a syringe. A fraction of the sample was taken as “whole cell lysate” for western blot analysis. The sample was centrifuged at maximum speed (21130 rcf) for 15 min at 4°C. The supernatant (“input”) was saved for western blot analysis. 100µl Dynabeads™ Protein G for Immunoprecipitation (magnetic, 10003D, Invitrogen) were washed with 1 ml 0.01% Tween-20/PBS. Beads were incubated with 3.5 µg mouse anti-GFP antibody (11814460001, Roche) for a minimum of 10 min on room temperature, rotating. After washing the beads twice with 1 ml 0.1% Tween-20/PBS and once with 1 ml RIPA buffer, beads were resuspended in RIPA buffer. The sample was incubated with antibody-conjugated Dynabeads over night at 4°C, rotating. Sample was pelleted and supernatant taken as “flow-through” for western blot analysis. The bead pellet was washed 3-5x with 1 ml RIPA buffer and twice with PBS, both freshly supplemented with 1x protease inhibitor. A fraction of the bead sample (“eluate”) was taken for western blot analysis. To prepare the sample for mass spectrometry analysis, PBS was exchanged by 100 µl 6 M Urea/ 50 mM ammonium bicarbonate (AB) and the sample was incubated with 2 µl of 50 mM reducing agent dithioerythritol/dH_2O for 1h at 37°C. After incubation of the sample with 2 µl of 400 mM alkylating agent iodoacetamide/ dH_2O for 1h in

the dark, the urea concentration was reduced to 1 M via addition of 500 µl AB. The sample was digested with 7 µl 0.1 µg/µl trypsin (Promega) /AB over night at 37°C. The supernatant was collected, dried completely using speed-vacuum and desalted with a C18 microspin column (Harvard Apparatus) according to the manufacturer's instructions. The sample was dried completely under speed-vacuum and stored at -20°C.

Mass spectrometry analysis and database search

The dried sample was dissolved in 20 µl loading buffer (5% acetonitrile, 0.1% formic acid). 2 µl of the sample were injected on column. LC-ESI-MS/MS was performed on a Q Q-Exactive HF Hybrid Quadrupole-Orbitrap Mass Spectrometer (Thermo Scientific) equipped with an Easy nLC 1000 liquid chromatography system (Thermo Scientific). Peptides were trapped on an Acclaim pepmap100, C18, 3µm, 75µm x 20mm nano trap-column (Thermo Scientific) and separated on a 75 µm x 250 mm, C18, 2µm, 100 Å Easy-Spray column (Thermo Scientific). For analytical separation, a gradient of 0.1% formic acid/H_2O (solvent A) and 0.1% formic acid/acetonitrile (solvent B) was run for 90 min at a flow rate 250 nl/min. The following gradient was used: 95 % A/5 % B for 0-5 min, 65 % A/35 % B for 60 min, 10 % A/90% B for 10 min and finally 10 % A/90 % B for 15 min. The MS1 full scan resolution was set to 60'000 full width half maximum (FWHM) at a mass/charge (m/z) ratio of 200 with an automatic gain control (AGC) target of 3 x 10^6 (number of ions), a maximum injection time of 60 ms and a mass range set to 400-2000 m/z. For data dependent analysis, up to twenty precursor ions were isolated and fragmented by higher-energy collisional dissociation at 27% normalized collision energy. MS2 scans were acquired in centroid mode with the resolution set to a FWHM of 15'000 at m/z 200 with an AGC target of 1 x 10^5 and a maximum injection time of 60 ms. Isolation width was set to 1.6 m/z. Full MS scans were acquired in profile mode. The dynamic exclusion was set to 20 s.

A peak list was generated from the raw data by using the conversion tool MS Convert (ProteoWizard). Files of the peaklist were searched against the Plasmo DB 3D7 database (release 46, 5548 entries) and combined with an in-house database containing common contaminants using Mascot (Matrix Science, version 2.5.1). For the Mascot search, trypsin was selected as the enzyme with one potential missed cleavage and tolerances of precursor ions and fragment ions were set to 10 ppm and 0.02 Da, respectively. Carbamidomethyl cysteine was set as fixed amino acid modification. Variable amino acid modifications were oxidized methionine, deaminated and phosphorylated serine, threonine, and tyrosine. For validation of the Mascot search, Scaffold 4.10.0 (Proteome Software) was used. The identified peptides were accepted when the probability to reach an FDR of less than 0.1% was higher than 44% with the Peptide Prophet algorithm [64] with Scaffold delta-mass correction. Protein identification was accepted when the probability was greater than 99% to reach a false discovery rate (FDR) of less than 1 % and when at least two peptides were

identified. Protein probabilities were assigned by the Protein Prophet algorithm [65]. Proteins with similar peptides that could not be differentiated based on MS/MS analysis alone were grouped to satisfy the principles of parsimony.

SDS Page and Western Blotting

Samples for western blot analysis taken during co-immunoprecipitation ("whole cell lysate", "flow-through", "input" and "eluate") were each supplemented with NuPAGE™ LDS Sample Buffer (4X) (NP0007, Invitrogen), 50 mM DTT and 5 % beta-mercaptoethanol. After sample incubation for 5 min at 95 °C, beads in the "eluate" sample were removed via a magnetic rack and only supernatant was used. Per lane, protein lysate of 1 x 10^7 cells was loaded on a 4-12% tris-glycine gel (Novex™WedgeWell™, XP04122BOX, Thermo Fisher Scientific) and run in tris-glycine buffer (25 mM Tris, 250 mM glycine, 0.1% SDS in H_2O). Proteins were transferred to a nitrocellulose membrane using the Mini Trans-Blot® Cell (1703930, Bio-Rad) system by blotting in tris-glycine based buffer (25 mM Tris, 192 mM glycine, 0.02% SDS, 0-25% methanol in deionized water), for 14 h at 40 mA on ice. All the following incubation steps of the membrane were performed at room temperature with slight agitation. First, the membrane was briefly rinsed in deionized water and incubated with Ponceau solution (0.1% (w/v) in 5% acetic acid, Ponceau S solution, P7170, Sigma-Aldrich) for 3-5 min. Second, it was briefly rinsed in deionized water and immediately imaged using the ChemiDoc XRS+ Gel Imaging System (Bio-Rad) equipped with the Image Lab 4.1 software. Next, the membrane was briefly incubated in deionized water and washed with 0.05% Tween-20/PBS. Nonspecific binding sites were blocked with 5 % milk powder/0.05% Tween-20/PBS for 30 min, exchanged again for blocking solution and incubated for another 15 min. The membrane was stained with primary antibody mouse anti-GFP in 5% milk powder/0.05% Tween-20/PBS for 1 h. After three washes with 0.05% Tween-20/PBS for 10 min, the membrane was stained with the secondary antibody goat anti-mouse IgGHRP in 5 % milk powder/0.05% Tween-20/PBS for 1h. After 3x 10 min washing steps with 0.05% Tween-20/PBS, the membrane was incubated with 1:1 Amersham ECL Prime Western Blotting Detection Reagent (RPN2232, Amersham) for 5 min and immediately imaged using the ChemiDoc system.

Samples for western blot analysis of tubulin and centrin abundance were taken of +/- 2.5h synchronized Slp parasites with or without 3.5mM GlcN after 24, 30 or 36 hpi by lysis in 0.15% saponin, followed by supplementation in 4X Laemmli buffer (1610747, Bio-Rad) and 2.5% beta-mercaptoethanol. Samples were incubated for 10 min at 95°C and lysate of 2*10^7, 1*10^7 and 2*10^6 cells was loaded for 24, 30 and 36 hpi respectively on a 4–15% Mini-PROTEAN® TGX™ Precast Protein Gel (4561083, Bio-Rad). Blotting was performed using the Trans-Blot Turbo Mini 0.2 µm Nitrocellulose Transfer Pack (1704158, Bio-Rad) on a Trans-Blot Turbo Transfer System (Bio-Rad). Thereafter, the membrane was blocked for 15 min in 5% milk powder in 0.5% Tween-20/PBS (5% milk). The blot was cut at the 25kDa

band, and the upper part was incubated with rabbit anti-PfAldolase and mouse anti-tubulin (Table S3), while the lower part was incubated with rabbit anti-Centrin3. Antibodies were always diluted in 5% milk, and staining occurred for 2h at Rt while shaking. The membrane was washed thrice for 10 min in 5% milk and incubated with anti-mouse 800CW and anti-rabbit 680R (upper part), or anti-rabbit 800CW (lower part) antibodies for 1h at RT shaking (Table S3). The blot was washed thrice in 5% milk for 10 min and once in PBS for 10 min before imaging on the LI-COR Odyssey® DLx Imaging System.

Generation of the pSLI_PfSlp-GFP-*glmS* plasmid

To generate the pSLI_PfSlp-GFP-*glmS* plasmid, pSLI-CRK4-GFP-*glmS* plasmid (kindly provided by Markus Ganter) was digested with NotI-HF and MluI-HF to remove the CRK4 sequence. PfSlp genomic sequence was amplified via PCR from NF54 genomic DNA (forward primer: TGACACTATAGAATACTCGCGGCCGCAGTGAAAAGACTGATGAAGG, reverse primer: CAGCAGCAGCACCTCTAGCACGCGTTTTTATCATGATAAGATTGTTAAGG). Ligation of backbone and PfSlp gene sequence was performed using Gibson assembly [66]. To verify the plasmid sequence, an analytical digest was performed followed by Sanger sequencing.

Parasite transfection

For transfection of 3D7 parasites with pSLI_PfSlp-GFP-*glmS*, 150 µl packed red blood cells infected with sorbitol-synchronized ring stages (~4% parasitemia) were mixed with 100 µg purified DNA in TE buffer and 300 µl prewarmed Cytomix (120 mM KCl, 0.15 mM CaCl2, 2 mM EGTA, 5 mM MgCl2, 10 mM K2HPO4/KH2PO4 pH 7.6, 25 mM HEPES pH 7.6). Parasite transfection was performed via electroporation using Gene Pulser II (Bio-Rad) at high capacity, 310 V and 950 µF. To select for transfected parasites, 2.5 nM WR99210 (Jacobus Pharmaceuticals) were added to the culture. Selection for construct integration was performed according to the protocol by Birnbaum et al., 2017 using 800 µg/ml Geneticin-G418 (Thermo Fisher Scientific). To check for correct integration, genomic DNA was extracted, and PCRs performed across the 5' and 3' integration site (Fig. S3). Primers used are found in Table S2.

Seeding of infected erythrocytes

For IFA, infected RBCs were seeded on eight-well chambered glass slides (glass bottom µ-Slide 8 Well, ibidi) by first coating the glass surface with Concanavalin A (Sigma-Aldrich, 5 mg/ml in ddH_2O) for 20 min at 37°C. For live-cell imaging, precoated 8 well slides (ibiTreat µ-Slide 8 Well, ibidi) were washed thrice briefly with prewarmed Dulbecco´s phosphate-buffered solution (PBS) (Gibco). Thereafter, the slides were rinsed thrice with prewarmed incomplete iRPMI 1640 medium. 150µl of infected erythrocyte culture per well was washed twice with incomplete RPMI and added to the coated slides. After letting the cells bind for at

least 10 min at 37°C unbound cells were removed via repeatedly shaking the slide and washing with 200µl iRPMI, until only a cell monolayer remained. Finally, cells were either incubated in 200µl complete medium at 37°C until live-cell imaging setup, or briefly rinsed with PBS before fixation in 4%PFA/PBS for 20 min at 37°C. Fixed cells were rinsed thrice with PBS before storage at 4°C or direct use for IFA.

Immunofluorescence assay

For IFA, seeded and PFA-fixed parasites were first permeabilized with 0.1%Triton-X-100/PBS for 15 minutes at RT and rinsed thrice with PBS. Afterwards, free aldehyde groups were quenched by incubation in fresh 0.1mg/ml $NaBH_4$ solution at RT for 10 min. After brief three-time rinsing, blocking was performed in 3% Bovine Serum Albumine (BSA) (Carl Roth) in PBS for 30 minutes. Primary antibodies targeting GFP, PfCentrin3 and tubulin were diluted to the according concentration in 3% BSA (Table S3) and incubated on the cells for 2h at RT while shaking. Primary antibodies were thereafter removed, and the dish was washed thrice with PBS-T for 10 min shaking before incubation with secondary antibodies and Hoechst (Table S3) for 90 min at RT. Cells were washed twice in PBS-T for 10 min, once in PBS and stored in PBS at 4°C until imaging.

Staining of infected red blood cells for live-cell imaging

For live cell imaging, Slp or 3D7 wt infected red blood cells (iRBCs) were seeded on dishes as described above. Cells were synchronized with sorbitol and treated with 3.5mM GlcN 24h before imaging. Imaging medium consisting of phenol red-free RPMI 1640 supplemented with L-Glutamine as well as the same supplements used in complete medium for culture was equilibrated in the cell culture incubator overnight. The live microtubule dye SPY555-Tubulin (Spirochrome) (Table S3) and 3.5mM GlcN were added into the imaging medium, and thereafter used for replacement of the culture medium of the seeded cells. The dish was closed airtight without residual air and incubated for 2h prior to imaging.

Confocal and STED microscopy

Confocal microscopy of fixed cells was performed on a Leica TCS SP8 scanning confocal microscope (Leica) with Lightning (LNG) automated adaptive deconvolution. Images were acquired using the HC PL APO CS2 63x/1.4 N.A. oil immersion objective, HyD detectors, and spectral emission filters. Brightfield images were obtained from a transmitted light PMT detector. In LNG mode, images were acquired using a pinhole of 0.5 airy units resulting in a pixel size of 29 nm and a total image size of 9.26 × 9.2 µm (320 × 320 pixels) with a pixel dwell time of 2.3µs. Z stacks were acquired at a total size of 6.27µm at a z-step size of 230 nm. STED microscopy was performed on a single-point scanning STED/RESOLFT super-resolution microscope (Abberior Instruments GmbH), equipped with a pulsed 775 nm STED depletion laser and three avalanche photodiodes for detection. Super-resolution images were

acquired using the 100× 1.4 NA objective, a pixel size of 20 nm and a pixel dwell time of 10 µs. The STED laser power was set to 5-15%, whereas the other lasers (405, 488, 594 and 640) were adjusted to the antibody combinations used (Table S3).

Live-cell imaging

Live-cell imaging was performed on a Zeiss LSM 900 microscope (Zeiss) equipped with the Airyscan detector using Plan-Apochromat 63x/1,4 oil immersion objective at 37℃ in a humidified environment. Movies were acquired at multiple positions using an automated stage and the Definite Focus module for focus stabilization with a time-resolution of 10 min for 18-21 h. Images were acquired sequentially in the sequence scanning mode using 567 nm diode lasers for SPY555-Tubulin imaging. Emission detection was configured using variable dichroic mirrors. Detectors were used with the gain adjusted between 700 and 900 V, offset was not adjusted (0%). Pinhole was set to 0.6 Airy Units. Brightfield images were obtained from a transmitted light PMT detector. Sampling was sized 19.11 µm x 19.11 µm at 50 nm pixel size xy bidirectionally with pixel dwell time between 0.7 and 1.2 µs without line averaging. Z-stacks of a total size of 6 µm at a z-step size of 350 nm were acquired. Subsequently, ZEN Blue 3.1 software was used for the 3D Airyscan processing with automatically determined default Airyscan Filtering (AF) strength. Trophozoites were identified in DIC and presence of a hemispindle was determined prior to imaging.

Image analysis and quantification

All graphs were plotted using Prism GraphPad. Statistical significance was determined via unpaired t-test with Welch´s correction. All images were analyzed using ImageJ [67]. If not stated otherwise, mean and SEM are plotted.

Representative images

Confocal images shown are maximum projections, brightness and contrast were adjusted in the same manner for +/- GlcN samples for visualization. Movie stills were acquired from maximum intensity projections with adjusted tubulin signal. Brightness and contrast of STED images were adjusted accordingly.

Centriolar plaque signal quantification

To determine the centrin and PfSlp intensity, maximum intensity projections of tubulin, centrin, PfSlp and DNA stained PfSlp parasites + (n=31) or - (n= 28) GlcN were acquired. Intensity of each signal was then measured using a circle with an area of 0.14µm^2 in ImageJ around the centrin/PfSlp signal. Extracellular and intracellular background was subtracted. Negative values were displayed as “0”. Determined signal (+GlcN (n=140), -GlcN (n=195) was plotted thereafter. Mean and SD shown.

Microtubule length determination

To calculate the average cumulative length of microtubule strands in hemispindles per nucleus, average intensity projections of tubulin, centrin, PfSlp and DNA stained Slp parasites +GlcN (n=31) or -GlcN (n=28) were acquired. Length of individual microtubule strands was then measured using the line tool in ImageJ. Length of each microtubule strand was cumulated for every hemispindle (+GlcN (n=66), -GlcN (n=73)).

Nuclear tubulin concentration

To calculate the average nuclear tubulin concentration in hemispindles and mitotic spindles, average intensity projections of tubulin, centrin, GFP stained PfSlp parasites + (n=31) or - (n= 28) GlcN were acquired. Intensity of each spindle was then measured using the polygon tool in ImageJ drawn around the tubulin signal. Intensity was divided by measured area to determine concentration after background subtraction. Concentration of hemispindles (+GlcN (n=70), -GlcN (n=89)) and mitotic spindles (+GlcN (n=38), -GlcN (n=64) was determined.

Western blot quantification

Protein band signal intensity was determined using Image Studio™. Centrin and tubulin levels were normalized to equal aldolase signal and corrected to display $2*10^7$ parasites.

Parasite spindle duration

To measure the duration of the first mitotic spindle, Slp (n=31) and 3D7 (n=20) parasites were previously treated with 3.5mM GlcN and movies were created as described above. Mitotic spindle duration was defined as first frame with identifiable mitotic spindle up to the last frame with identifiable mitotic spindle.

Live cell microscopy microtubule concentration

To measure the duration of the first mitotic spindle, movies of Slp (n=29) and 3D7 (n=19) parasites previously treated with 3.5mM GlcN or untreated Slp parasites were created as described above. Average intensity projections of z-slides containing the mitotic spindle at the first time frame with identifiable mitotic spindle. Microtubule intensity was then measured using a circle tool in ImageJ drawn around the mitotic spindle. Intracellular background was subtracted. Mean and SD are shown.

Percentage of failed anaphase spindles

Relative failure to extend the anaphase spindle was determined by creation of live cell data as described above. Failure was defined as multiple extension attempts without severing of the anaphase microtubule strands. Slp +GlcN (n=36), Slp -GlcN (18), 3D7 +GlcN (n=20).

Parasite growth assay

Synchronized PfSlp and 3D7 parasites were treated with +/- 3.5mM GlcN. Growth assay was performed as described previously [18]. 100µl resuspended medium were taken and fixed with 4% PFA/PBS and 0.0075% Glutaraldehyde for 30 min at RT every 24 hpi. Samples were washed, permeabilized with Triton™ X–100 (Sigma, T8787) for 8 min and treated with 0.3mg/ml Ribonuclease A (Sigma, R4642) in PBS for 30 min. Cells were washed twice and

resuspended in 100µl staining solution (1:2000 SYBR green I (Invitrogen) in PBS) followed by 20 min incubation. After subsequent washing cells were diluted to the preferred dilution and parasitemia was determined via flow cytometry. Cells were gated for single red blood cells and plotted using Prism Graphpad. N=3

Merozoite quantification

To quantify the average number of merozoites per segmenter, sorbitol synchronized PfSlp-GFP and wt 3D7 parasites were treated with 50µM of the egress inhibiting protease inhibitor trans-epoxysuccinyl-L-leucylamido (4-guanidino) butane (E64) after 33h or 74h of treatment with Glucosamine as early ring stage parasites. Untreated cells of both strains served as control. After 4 hours E64 incubation, number of merozoites per late stage schizont was determined via giemsa smear. Statistical significance was determined using unpaired two-sided student's t-test via Prism GraphPad software.

RT-qPCR

To determine the PfSlp RNA abundance upon knockdown, iRBCs +/- 3.5 mM GlcN were first lysed using 0.15% Saponin in PBS. Thereafter RNA was extracted using the NucleoSpin RNA kit (Macherey-Nagel, 740955.50) and cDNA was synthesized *in vitro* using the RevertAid first strand cDNA synthesis kit (Thermo Fisher, K1622). qPCR was performed using SYBR-green with primers targeting the PfSlp cDNA and t-serine ligase as housekeeping control. Knockdown was determined using the delta-delta method with averaged housekeeping genes throughout all replicas. Statistical significance was determined using Prism GraphpPad. N=3.

Determination of S-Phase onset via flow cytometry

For analysis of parasite replication via flow cytometry cells were first synchronized using quadroMACS™ (Miltenyi Biotec) magnetic purification of late stage schizonts followed by sorbitol treatment after 2h. iRBCs with a Parasitemia of ~0.5% were thereafter treated with 3.5mM GlcN or left untreated and incubated at the beforementioned incubation conditions, after 24 hpi 200µl of medium was taken and fixed with 4%PFA/PBS and 0.0075% Glutaraldehyde for 12h at 4°C every 6h until 48 hpi. Samples were washed, permeabilized with Triton™ X–100 (Sigma, T8787) for 8 min and treated with 0.3mg/ml Ribonuclease A (Sigma, R4642) in PBS for 30 min. Cells were washed twice and resuspended in 100µl staining solution (1:2000 SYBR green I in PBS) followed by 20 min incubation. After subsequent washing cells were diluted to the preferred dilution and DNA content was analyzed via flow cytometry. Cells were gated for 2000 single, infected red blood cells and SYBR green emission intensity after FITC excitation was measured for each time point and condition. Intensity was normalized for the highest emission in each individual experiment and plotted using Prism GraphPad. N=3.

Conflicts of Interest

none declared

Author Contributions

C.S.S., C.W. and J.G. planned and designed the study. C.S.S. carried out co-immunoprecipitation and mass spectrometry analysis under the supervision of N.K. and M.B. T.P.R. and C.S.S. tagged PfSlp. C.W. validated the knock down. Growth curve was generated by M.M. with help by T.P.R. All further localization and phenotypic analysis were done by C.W. with help from J.G. for STED, from A.K. for flow cytometry of DNA content, from V.S. for live cell imaging, and from Y.V. for western blotting and the PfCen1-GFP line. J.G. and C.W. compiled the figures with help by C.S.S. and M.M. J.G. and C.W. and wrote the text. C.S.S., M.G. and M.B. reviewed and edited the text and figures.

Funding

We thank the German Research Foundation (DFG) (349355339), the Human Frontiers Science Program (CDA00013/2018-C), the Daimler and Benz Foundation, and the Chica and Heinz Schaller Foundation for funding to J.G. The “Studienstiftung des Deutschen Volkes” for funding to Y.V. The “Landesgraduierteförderung Baden-Württemberg” for funding to C.S.S. The German Research Foundation (DFG) – Project number 240245660 - SFB 1129 and the Baden-Württemberg Foundation (1.16101.17) for funding to M.G, as well as the Fundação para a Ciência e Tecnologia (FCT, Portugal) - PD/BD/128002/2016 to M.M. Collaborative work between the laboratories of J.G. and M.B. was possible with the support of an EMBO short-term fellowship (8314) to C.S. Work in M.B. laboratory is supported by the Swiss National Science Foundation (31003A_179321 and 310030_208151).

Acknowledgments

We thank: The Infectious Diseases Imaging Platform for imaging support (idip-heidelberg.org). The Instituto Aggeu Magalhães- Fundação Oswaldo Cruz- FIOCRUZ/PE for the collaboration during the sabbatical period of Dr. Tatiany Romão at our Center. PlasmoDB for their Plasmodium Informatics Resources (plasmodb.org). Nicolas Lichti for help with molecular cloning. The MSc students of the Major Infectious Diseases that participated in the practical course on Pathogenic Microorganisms 2021 for generating preliminary imaging data. The excellent service at the proteomic core facility at the Faculty of Medicine of the University of Geneva.

References

1. WHO (2021) *WHO Global, World Malaria Report 2021*.
2. Francia ME, Striepen B (2014) Cell division in apicomplexan parasites. *Nat Rev Microbiol* **12**: 125–136.
3. Gerald N, Mahajan B, Kumar S (2011) Mitosis in the human malaria parasite plasmodium falciparum. *Eukaryot Cell* **10**: 474–482.
4. Simon CS, Stürmer VS, Guizetti J (2021) How Many Is Enough? - Challenges of Multinucleated Cell Division in Malaria Parasites. *Front Cell Infect Microbiol* **11**: 658616.
5. Mancio-Silva L, Slavic K, Grilo Ruivo MT, Grosso AR, Modrzynska KK, Vera IM, Sales-Dias J, Gomes AR, Macpherson CR, Crozet P, et al. (2017) Nutrient sensing modulates malaria parasite virulence. *Nature* **547**: 213–216.
6. Kumar M, Skillman K, Duraisingh MT (2021) Linking nutrient sensing and gene expression in Plasmodium falciparum blood-stage parasites. *Mol Microbiol* **115**: 891–900.
7. Schofield L (2007) Intravascular infiltrates and organ-specific inflammation in malaria pathogenesis. *Immunol Cell Biol* **85**: 130–137.
8. White MW, Suvorova ES (2018) Apicomplexa Cell Cycles: Something Old, Borrowed, Lost, and New. *Trends Parasitol* **34**: 759–771.
9. Gubbels MJ, Coppens I, Zarringhalam K, Duraisingh MT, Engelberg K (2021) The Modular Circuitry of Apicomplexan Cell Division Plasticity. *Front Cell Infect Microbiol* **11**: 670049.
10. Klaus S, Binder P, Kim J, Machado M, Funaya C, Schaaf V, Klaschka D, Kudulyte A, Cyrklaff M, Laketa V, et al. (2022) Asynchronous nuclear cycles in multinucleated Plasmodium falciparum facilitate rapid proliferation. *Sci Adv* **8**: 1–13.
11. McDonald J, Merrick CJ (2021) DNA replication dynamics during erythrocytic schizogony in the malaria parasites Plasmodium falciparum and Plasmodium knowlesi. *bioRxiv* 2021.12.20.473505.
12. Liffner B, Absalon S (2021) Expansion Microscopy Reveals Plasmodium falciparum Blood-Stage Parasites Undergo Anaphase with A Chromatin Bridge in the Absence of Mini-Chromosome Maintenance Complex Binding Protein. *Microorganisms* **9**: 2306.
13. Gubbels MJ, Keroack CD, Dangoudoubiyam S, Worliczek HL, Paul AS, Bauwens C, Elsworth B, Engelberg K, Howe DK, Coppens I, et al. (2020) Fussing About Fission: Defining Variety Among Mainstream and Exotic Apicomplexan Cell Division Modes. *Front Cell Infect Microbiol* **5**: 269.
14. Guttery DS, Poulin B, Ramaprasad A, Wall RJ, Ferguson DJP, Brady D, Patzewitz EM, Whipple S, Straschil U, Wright MH, et al. (2014) Genome-wide functional analysis of plasmodium protein phosphatases reveals key regulators of parasite development and differentiation. *Cell Host Microbe* **16**: 128–140.
15. Morahan BJ, Abrie C, Al-Hasani K, Batty MB, Corey V, Cowell AN, Niemand J, Winzeler EA, Birkholtz LM, Doerig C, et al. (2020) Human Aurora kinase inhibitor Hesperadin reveals epistatic interaction between Plasmodium falciparum PfArk1 and PfNek1 kinases. *Commun Biol* **3**: 1–10.
16. Reininger L, Wilkes JM, Bourgade H, Miranda-Saavedra D, Doerig C (2011) An essential Aurora-related kinase transiently associates with spindle pole bodies during Plasmodium falciparum erythrocytic schizogony. *Mol Microbiol* **79**: 205–221.
17. Tewari R, Straschil U, Bateman A, Böhme U, Cherevach I, Gong P, Pain A, Billker O (2010) The systematic functional analysis of plasmodium protein kinases identifies essential regulators of mosquito transmission. *Cell Host Microbe* **8**: 377–387.
18. Ganter M, Goldberg JM, Dvorin JD, Paulo JA, King JG, Tripathi AK, Paul AS, Yang J, Coppens I, Jiang RHY, et al. (2017) Plasmodium falciparum CRK4 directs continuous rounds of DNA replication during schizogony. *Nat Microbiol* **2**: 17017-.
19. Robbins JA, Absalon S, Streva VA, Dvorin JD (2017) The Malaria Parasite Cyclin H Homolog PfCyc1 Is Required for Efficient Cytokinesis in Blood-Stage Plasmodium falciparum. *MBio* **8**: e00605-17.
20. Balestra AC, Zeeshan M, Rea E, Pasquarello C, Brusini L, Mourier T, Subudhi AK, Klages N, Arboit P, Pandey R, et al. (2020) A divergent cyclin/cyclin-dependent kinase complex controls the atypical replication of a malaria parasite during gametogony and transmission. *Elife* **9**: 1–25.
21. Rieder CL (2011) Mitosis in vertebrates: The G2/M and M/A transitions and their associated checkpoints. *Chromosom Res* **19**: 291–306.
22. Musacchio A, Salmon ED (2007) The spindle-assembly checkpoint in space and time. *Nat Rev Mol Cell Biol* **8**: 379–393.

23. Matthews H, Duffy CW, Merrick CJ (2018) Checks and balances? DNA replication and the cell cycle in Plasmodium. *Parasites and Vectors* **11**: 216.
24. Brusini L, Santos Pacheco N Dos, Soldati-Favre D, Brochet M (2021) Organization and composition of apicomplexan kinetochores reveal plasticity in chromosome segregation across parasite modes of division. *bioRxiv* 2021.11.03.466924.
25. Naughton JA, Bell A (2007) Studies on cell-cycle synchronization in the asexual erythrocytic stages of Plasmodium falciparum. *Parasitology* **134**: 331–337.
26. Absalon S, Dvorin JD (2021) Depletion of the mini-chromosome maintenance complex binding protein allows the progression of cytokinesis despite abnormal karyokinesis during the asexual development of Plasmodium falciparum. *Cell Microbiol* **23**: e13284.
27. Fu J, Hagan IM, Glover DM (2015) The centrosome and its duplication cycle. *Cold Spring Harb Perspect Med* **7**: a015800.
28. Carvalho-Santos Z, Machado P, Branco P, Tavares-Cadete F, Rodrigues-Martins A, Pereira-Leal JB, Bettencourt-Dias M (2010) Stepwise evolution of the centriole-assembly pathway. *J Cell Sci* **123**: 1414–1426.
29. Suvorova ES, Francia M, Striepen B, White MW (2015) A novel bipartite centrosome coordinates the apicomplexan cell cycle. *PLoS Biol* **13**: e1002093.
30. Tomasina R, González F, Francia ME (2021) *Structural and Functional Insights into the Microtubule Organizing Centers of Toxoplasma gondii and Plasmodium spp*.
31. Arnot DE, Ronander E, Bengtsson DC (2011) The progression of the intra-erythrocytic cell cycle of Plasmodium falciparum and the role of the centriolar plaques in asynchronous mitotic division during schizogony. *Int J Parasitol* **41**: 71–80.
32. Mehnert AK, Simon CS, Guizetti J (2019) Immunofluorescence staining protocol for STED nanoscopy of Plasmodium-infected red blood cells. *Mol Biochem Parasitol* **229**: 47–52.
33. Read M, Sherwin T, Holloway SP, Gull K, Hyde JE (1993) Microtubular organization visualized by immunofluorescence microscopy during erythrocytic schizogony in Plasmodium falciparum and investigation of post-translational modifications of parasite tubulin. *Parasitology* **106**: 223–232.
34. Simon CS, Funaya C, Bauer J, Voβ Y, Machado M, Penning A, Klaschka D, Cyrklaff M, Kim J, Ganter M, et al. (2021) An extended DNA-free intranuclear compartment organizes centrosome microtubules in malaria parasites. *Life Sci Alliance* **4**: e202101199.
35. Bertiaux E, Balestra A, Bournonville L, Brochet M, Guichard P, Hamel V (2021) Expansion Microscopy provides new insights into the cytoskeleton of malaria parasites including the conservation of a conoid. *PLoS Biol* **19**: e3001020.
36. Mahajan B, Selvapandiyan A, Gerald NJ, Majam V, Zheng H, Wickramarachchi T, Tiwari J, Fujioka H, Moch JK, Kumar N, et al. (2008) Centrins, cell cycle regulation proteins in human malaria parasite Plasmodium falciparum. *J Biol Chem* **283**: 31871–31883.
37. Roques M, Stanway RR, Rea EI, Markus R, Brady D, Holder AA, Guttery DS, Tewari R (2019) Plasmodium centrin Pb CEN-4 localizes to the putative MTOC and is dispensable for malaria parasite proliferation. *Biol Open* **8**: bio036822.
38. Salisbury JL (2007) A mechanistic view on the evolutionary origin for centrin-based control of centriole duplication. *J Cell Physiol* **213**: 420–428.
39. Dantas TJ, Daly OM, Morrison CG (2012) Such small hands: The roles of centrins/caltractins in the centriole and in genome maintenance. *Cell Mol Life Sci* **69**: 2979–2997.
40. Rüthnick D, Vitale J, Neuner A, Schiebel E (2021) The N-terminus of Sfi1 and yeast centrin Cdc31 provide the assembly site for a new spindle pole body. *J Cell Biol* **220**: e202004196.
41. Li S, Sandercock AM, Conduit P, Robinson C V., Williams RL, Kilmartin J V. (2006) Structural role of Sfi1p-centrin filaments in budding yeast spindle pole body duplication. *J Cell Biol* **173**: 867–877.
42. Bouhlel IB, Laporte MH, Bertiaux E, Giroud A, Borgers S, Azimzadeh J, Bornens M, Guichard P, Paoletti A, Hamel V (2021) SFI1 and centrin form a distal end complex critical for proper centriole architecture and ciliogenesis. *bioRxiv* 2021.10.05.463184.
43. Zeeshan M, Brady D, Stanway RR, Moores CA, Holder AA, Tewari R (2020) Plasmodium berghei Kinesin-5 Associates With the Spindle Apparatus During Cell Division and Is Important for Efficient Production of Infectious Sporozoites. *Front Cell Infect Microbiol* **10**: 583812.
44. Zeeshan M, Shilliday F, Liu T, Abel S, Mourier T, Ferguson DJP, Rea E, Stanway RR, Roques M, Williams D, et al. (2019) Plasmodium kinesin-8X associates with mitotic spindles and is essential for oocyst development during parasite proliferation and transmission. *PLoS Pathog* **15**: e100804.
45. Mitchison T, Kirschner M (1984) Dynamic instability of microtubule growth. *Nature* **312**: 237–242.
46. Hirst WG, Fachet D, Kuropka B, Weise C, Saliba KJ, Reber S (2022) Purification of functional

Plasmodium falciparum tubulin allows for the identification of parasite-specific microtubule inhibitors. *Curr Biol* **32**: 919-926.e6.

47. Woodruff JB, Ferreira Gomes B, Widlund PO, Mahamid J, Honigmann A, Hyman AA (2017) The Centrosome Is a Selective Condensate that Nucleates Microtubules by Concentrating Tubulin. *Cell* **169**: 1066-1077.e10.
48. Balestra AC, Koussis K, Klages N, Howell SA, Flynn HR, Bantscheff M, Pasquarello C, Perrin AJ, Brusini L, Arboit P, et al. (2021) *Ca 2+ signals critical for egress and gametogenesis in malaria parasites depend on a multipass membrane protein that interacts with PKG*.
49. Zhang M, Wang C, Otto TD, Oberstaller J, Liao X, Adapa SR, Udenze K, Bronner IF, Casandra D, Mayho M, et al. (2018) Uncovering the essential genes of the human malaria parasite Plasmodium falciparum by saturation mutagenesis. *Science* **360**: eaap7847.
50. Gogendeau D, Beisson J, De Loubresse NG, Le Caer JP, Ruiz F, Cohen J, Sperling L, Koll F, Klotz C (2007) An Sfi1p-like centrin-binding protein mediates centrin-based Ca 2+-dependent contractility in Paramecium tetraurelia. *Eukaryot Cell* **6**: 1992–2000.
51. Birnbaum J, Flemming S, Reichard N, Soares AB, Mesén-Ramírez P, Jonscher E, Bergmann B, Spielmann T (2017) A genetic system to study Plasmodium falciparum protein function. *Nat Methods* **14**: 450–456.
52. Prommana P, Uthaipibull C, Wongsombat C, Kamchonwongpaisan S, Yuthavong Y, Knuepfer E, Holder AA, Shaw PJ (2013) Inducible knockdown of Plasmodium gene expression using the glmS ribozyme. *PLoS One* **8**: e73783.
53. Charnaud SC, Kumarasingha R, Bullen HE, Crabb BS, Gilson PR (2018) Knockdown of the translocon protein EXP2 in Plasmodium falciparum reduces growth and protein export. *PLoS One* **13**: 1–14.
54. LaCount DJ, Vignali M, Chettier R, Phansalkar A, Bell R, Hesselberth JR, Schoenfeld LW, Ota I, Sahasrabudhe S, Kurschner C, et al. (2005) A protein interaction network of the malaria parasite Plasmodium falciparum. *Nature* **438**: 103–107.
55. Ito D, Bettencourt-Dias M (2018) Centrosome remodelling in evolution. *Cells* **7**: 71.
56. Rüthnick D, Schiebel E (2016) Duplication of the Yeast Spindle Pole Body Once per Cell Cycle. *Mol Cell Biol* **36**: 1324–1331.
57. Kilmartin J V. (2003) Sfi1p has conserved centrin-binding sites and an essential function in budding yeast spindle pole body duplication. *J Cell Biol* **162**: 1211–1221.
58. Avena JS, Burns S, Yu Z, Ebmeier CC, Old WM, Jaspersen SL, Winey M (2014) Licensing of Yeast Centrosome Duplication Requires Phosphoregulation of Sfi1. *PLoS Genet* **10**: e100466.
59. De Souza CPC, Osmani SA (2007) Mitosis, not just open or closed. *Eukaryot Cell* **6**: 1521–1527.
60. Boettcher B, Barral Y (2013) The cell biology of open and closed mitosis. *Nucleus* **4**:.
61. Pavin N, Tolić IM (2016) Self-Organization and Forces in the Mitotic Spindle. *Annu Rev Biophys* **45**: 279–298.
62. Hawkins LM, Naumov A V, Batra M, Wang C, Chaput D, Suvorova ES (2022) Novel CRK-Cyclin Complex Controls Spindle Assembly Checkpoint in Toxoplasma Endodyogeny. *MBio* **13**: e03561-21.
63. Fang H, Klages N, Baechler B, Hillner E, Yu L, Pardo M, Choudhary J, Brochet M (2017) Multiple short windows of calcium-dependent protein kinase 4 activity coordinate distinct cell cycle events during Plasmodium gametogenesis. *Elife* **6**: 1–23.
64. Keller A, Nesvizhskii AI, Kolker E, Aebersold R (2002) Empirical Statistical Model To Estimate the Accuracy of Peptide Identifications Made by MS/MS and Database Search. *Anal Chem* **74**: 5383–5392.
65. Nesvizhskii AI, Keller A, Kolker E, Aebersold R (2003) A Statistical Model for Identifying Proteins by Tandem Mass Spectrometry. *Anal Chem* **75**: 4646–4658.
66. Gibson DG, Young L, Chuang RY, Venter JC, Hutchison CA 3rd, Smith HO (2009) Enzymatic assembly of DNA molecules up to several hundred kilobases. *Nat Methods* **6**: 343–345.
67. Schindelin J, Arganda-Carreras I, Frise E, Kaynig V, Longair M, Pietzsch T, Preibisch S, Rueden C, Saalfeld S, Schmid B, et al. (2012) Fiji: An open-source platform for biological-image analysis. *Nat Methods* **9**: 676–682.